Structural and dielectric properties of sol–gel processed Ce-doped BaTi$_{0.97}$Y$_{0.03}$O$_3$ ceramics

Aziz Nfissi*, Yahya Ababou*,‡, Mounir Belhajji*, Salaheddine Sayouri*
and Taj-dine Lamcharfi†

*LPAIS, Faculty of Sciences-DM, USMBA, B.P. 1796, Fez-Atlas, Morocco

†LSSC, Faculty of Sciences and Technology, Street Immouzar, B. P. 2202, Fez, Morocco

‡ababouyahya@hotmail.com

Structural and dielectric properties of Ce-doped BaTi$_{0.97}$Y$_{0.03}$O$_3$ powders, with the chemical formulation (Ba$_{1-x}$Ce$_x$)(Ti$_{(0.97-x/4)}$-Y$_{0.03}$)O$_3$ such as x = 0%, 1%, 3%, 5%, 7% and 9%, produced by the sol–gel method, have been investigated. X-ray diffraction analysis showed that Ce^{3+} ions incorporated Ba sites until x = 7% indicating that this concentration represents a solubility limit of Ce^{3+} ions in BaTi$_{0.97}$Y$_{0.03}$O$_3$ matrix. Scanning electron microscopy (SEM) analysis showed a decrease in grain size down to the same concentration of 7%. Raman spectroscopy analysis showed the appearance of A$_{1g}$ mode, which we attributed to the effect of incorporation of Ce^{3+} and Y^{3+} in BaTiO$_3$ matrix. Dielectric measurements revealed that doping with cerium lowers the temperature of permittivity maximum at the ferroelectric-to-paraelectric transition (FPT) of the BaTi$_{0.97}$Y$_{0.03}$O$_3$ sample, and reaches a value that should be below 40 °C for x = 9%. Moreover, the phenomenon of dielectric resonance was observed on all Ce-doped samples, which was not the case with other dopants as reported in the literature.

Keywords: Ce-doped BaTi$_{0.97}$Y$_{0.03}$O$_3$; sol–gel process; dielectric properties; FPT temperature; resonance.

1. Introduction

Ceramic compounds with high dielectric constant and low dielectric loss offer many technological applications such as high energy storage devices, multilayer ceramic capacitors (MLCCs), actuators, memory devices, sensors, etc.[1–2] In this regard, Barium Titanate (BaTiO$_3$) is a potential candidate among other ceramic materials. It has dielectric, piezoelectric and ferroelectric properties with ferro-to-paraelectric transition temperature (FPT) at around 130 °C.[3] Unfortunately, the latter is high, which limits its application in electronic devices, particularly in MLCC devices. However, it is possible to improve physical properties of this material by substitutions on Ba-site, Ti-site or on both sites (co-doping).[4–7] It has been shown that the incorporation of rare earth elements (RE = Sm, Nd, La) in BaTiO$_3$ ceramics lowers its FPT temperature (T_c).[8–10] For example, the rate of decrease in T_c is 25 °C/mol% of La^{3+} doped at Ba-site[11] and 20 °C/mol% of Ho^{3+} doped at Ti-site.[12] Indeed, the ionic radius of the RE elements is very important to know which site they will occupy. The RE with large ionic radius (r(RE) > 0.94 Å) such as Ce^{3+} will occupy Ba^{2+} site and act as donors, whereas the RE with small ionic radius (r(RE) < 0.87 Å) such as Yb^{3+} will occupy Ti^{4+} site and act as acceptors with charge compensation by oxygen vacancies.[13,14] On the other hand, the RE with intermediate ionic radii (0.87 Å < r(RE) < 0.94 Å) such as Y^{3+} can occupy Ba^{2+} and/or Ti^{4+} sites in BaTiO$_3$[15] which depends on the Ba/Ti ratio.[16]

The ionic radius of all RE elements is larger than that of Ti^{4+} (r(Ti^{4+}) = 0.605 Å) (Table 1), but is smaller than that of Ba^{2+} (r(Ba^{2+}) = 1.61 Å). Therefore, a substitution of Ti^{4+} site by RE^{3+} ions results in an expansion of the volume of the unit cell in BaTiO$_3$ matrix, whereas a substitution of Ba^{2+} by RE^{3+} ions leads to a shrinkage of this volume.[17]

In the present work, we studied the effect of Cerium on structural and dielectric properties of sol–gel processed BaTi$_{0.97}$Y$_{0.03}$O$_3$ ceramics.

2. Experiment

2.1. Samples preparation

A series of Ce-doped BaTi$_{0.97}$Y$_{0.03}$O$_3$ samples, (Ba$_{1-x}$Ce$_x$)-(Ti$_{(0.97-x/4)}$Y$_{0.03}$)O$_3$ (denoted BCYTx), was prepared by the sol–gel process which is schematized in Fig. 1. During the preparation process: Titanium isopropoxide, Barium acetate trihydrate, Cerium (III) acetate hydrate and Yttrium (III) acetate hydrate were used as precursors. Lactic acid was used as peptizing agent and distilled water was used as solvents. The raw powders were calcined at 950 °C for 4 h in a programmable oven. For dielectric measurements, the

‡Corresponding author.

Table 1.   Ionic radii for some rare earth ions (coordination number = 6).[18]

RE	Large ionic radius			Intermediate ionic radius					Small ionic radius	
	La^{3+}	Ce^{3+}	Nd^{3+}	Gd^{3+}	Dy^{3+}	Ho^{3+}	Y^{3+}	Er^{3+}	Yb^{3+}	Lu^{3+}
$r(RE)$ (Å)	1.032	1.01	0.983	0.938	0.912	0.901	0.90	0.89	0.868	0.861
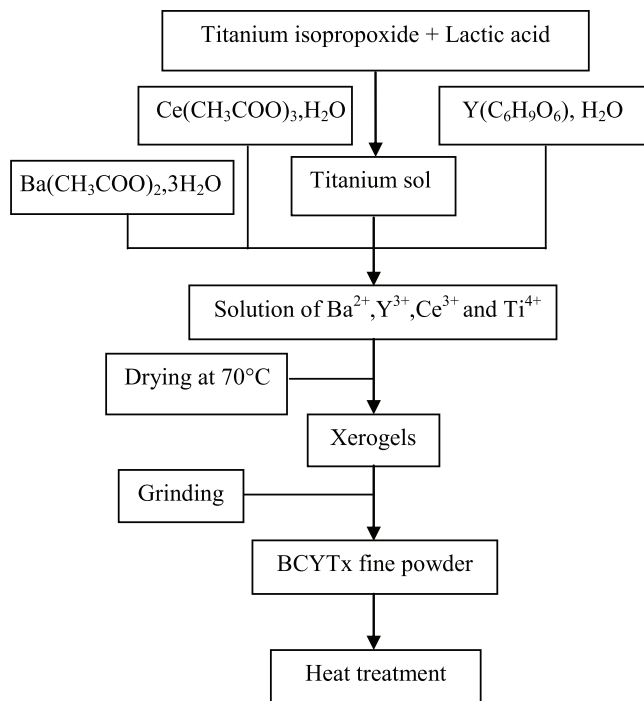
Fig. 1.   Flowchart of the preparation of BCYT*x* samples.

calcined powders were uniaxially pressed into pellets and were sintered at 1200 °C for 6 h.

2.2. *Samples characterization*

The structural properties of the samples were investigated by X-ray diffraction with Cu-Kα radiation λ = 1.54059 Å (diffractometer XPERT-PRO) and Raman spectroscopy (Senterra dispersive Raman microscope). The microstructural properties of the ceramics were investigated using a scanning electron microscope (SEM) (quanta 200 FEI). The dielectric measurements were performed in the frequency (500 Hz–2 MHz) and temperature ranges (ambient–300 °C) using an impedance analyzer (Agilent 4284A).

3.   Results and Discussion

3.1.   *Structural analysis*

Figure 2(a) shows the XRD patterns of the as-prepared $(Ba_{1-x}Ce_x)(Ti_{(0.97-x/4)}Y_{0.03})O_3$ samples (BCYT*x*, *x* = 0%, 1%, 3%, 5%, 7% and 9%), calcined at 950 °C for 4 h. It can be

seen that, at room temperature, all the samples have the pseudo-cubic structure with the presence of $BaCeO_3$ secondary phase for concentrations greater than 3%.

Lu *et al.*[19] prepared $(Ba_{1-x}Ce_x)(Ti_{0.95-x/4}Ce_{0.05})O_3$ (1% ≤ *x* ≤ 5%) samples using the mixed oxide method and have observed a pseudo-cubic structure for *x* = 3%, and have noticed the presence of a small amount of $BaCeO_3$ and CeO_2 for all concentrations.

A zoom in on the peak (110) (Fig. 2(b)) in the range 30.7° < 2θ < 32.2° shows a shift of this peak first towards higher angles for the concentrations *x* ≤ 7% in cerium. Values of the corresponding diffraction angles as a function of Ce^{3+} concentration are presented in Table 2.

The observed shift to higher angles for the concentrations *x* ≤ 7% in cerium indicates a shrinkage of the volume (*V*) of
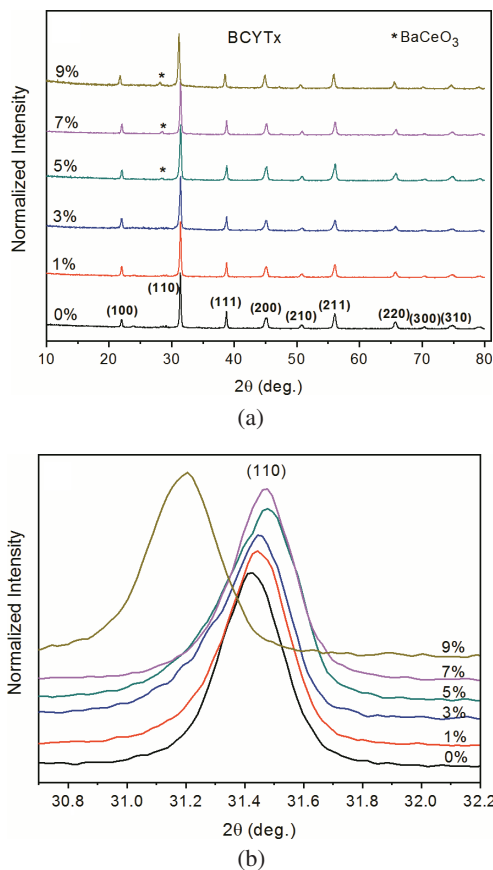

Fig. 2.   (a) XRD patterns of BCYT*x* samples. (b) Shifting of the peak (110).

Table 2. Variation of the position of the peak (110).

x (%)	Position (2θ) of the peak (110)
0	31.4218
1	31.4363
3	31.4453
5	31.4505
7	31.4595
9	31.1887

the unit cell. Indeed, since the ionic radius of $Ce^{3+}(r(Ce^{3+}) = 1.34$ Å, coordination number (CN) = 12) is smaller than that of $Ba^{2+}(r(Ba^{2+}) = 1.61$ Å, CN = 12), a substitution of Ba^{2+} ions by Ce^{3+} ones in $BaTi_{0.97}Y_{0.03}O_3$ matrix results in a shrinkage of the volume of the unit cell. Moreover, the peak shifting to lower angles for the concentrations $x > 7\%$ in cerium indicates an expansion of this volume (Table 4), since the ionic radius of Ce^{3+} $(r(Ce^{3+}) = 1.01$ Å, CN = 6) is larger than that of $Ti^{4+}(r(Ti^{4+}) = 0.605$Å, CN = 6), which indicates that the concentration $x = 7\%$ represents a solubility limit of Ce^{3+} ions in $BaTi_{0.97}Y_{0.03}O_3$ matrix.

The Goldschmidt tolerance factor, t, is extensively used to predict the stability of the perovskite structure based only on the chemical formula, ABO_3, and the ionic radii r_A, r_B and r_O of A and B site ions and the O-ion, respectively. In general, the perovskite structure will be formed if the value of the parameter t is close to one. t is given by the following equation:

$$t = [r_A + r_O]/[\sqrt{2}(r_B + r_O)]. \tag{1}$$

Table 3 shows the calculated values of the tolerance factor, t, of BCYTx samples using Eq. (1).

Values of t for the doped samples are slightly different from that of the pure $BaTiO_3$ ($t = 1.06$) as a consequence of incorporation of dopants of lower ionic radius.

Table 4 gives the values of the lattice parameters, tetragonality, unit cell volume and average crystallite size of BCYTx.

The observed evolution of the lattice parameters, in particular the decrease of the parameter c/a, as a function of Ce content (x) indicates a tendency towards the pseudo-cubic phase.

Table 3. Tolerance factor of the as-prepared BCYTx samples.

x (%)	t
0	1.056
1	1.056
3	1.054
5	1.052
7	1.050
9	1.048

Table 4. Lattice parameters, tetragonality, unit cell volume and average crystallite size of BCYTx.

x (%)	Lattice parameters		Tetragonality	Volume (Å³)	Average crystallite size (nm)
	a (Å)	c (Å)	(c/a)		
0	4.0096	4.0114	1.00044	64.4908	22.9479
1	4.0089	4.0100	1.00027	64.4458	22.3883
3	4.0085	4.0093	1.00019	64.4217	20.4184
5	4.0078	4.0085	1.00017	64.3863	20.1546
7	4.0074	4.0080	1.00014	64.3655	19.5956
9	4.0396	4.0400	1.00009	65.9262	23.3915

The average crystallite size of BCYTx samples was estimated using Scherrer's equation from the full-width-at-half-maximum (FWHM) of all diffraction peaks:

$$D = (0.9*\lambda)/(\beta *\cos\theta). \tag{2}$$

In this equation, λ, β and θ refer to the X-ray wave length (1.5406 Å), the FWHM of a characteristic diffraction peak and the diffraction angle, respectively.

The evolution of the average crystallite size as a function of x is displayed in Fig. 3, and Table 4 gives their values. They show a decrease in the average crystallite size as a function of x up to 7%, followed by an increase. This minimum recorded at $x = 7\%$ is in agreement with the previous results relating to the deformation of the unit cell for this same value, and which can be attributed to the solubility limit of Ce^{3+} ions that is reached for this concentration of 7% in the $BaTi_{0.97}Y_{0.03}O_3$ matrix.

3.2. *Raman analysis*

Raman spectra, recorded at room temperature (RT), of the $(Ba_{1-x}Ce_x)(Ti_{(0.97-x/4)}Y_{0.03})O_3$ (x = 0%, 1%, 3%, 5%, 7%
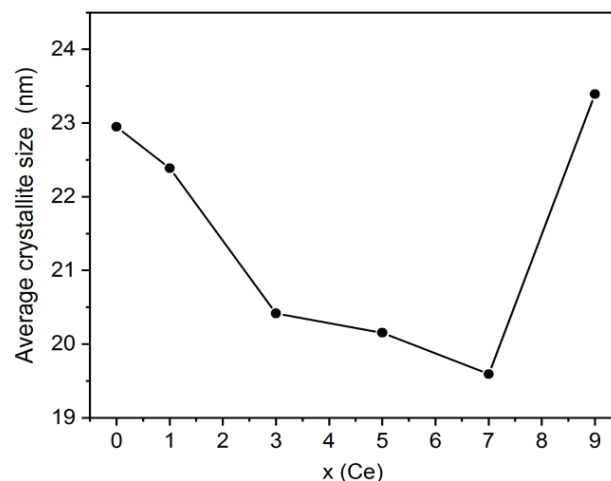
Fig. 3. Evolution of the average crystallite size of BCYTx samples.

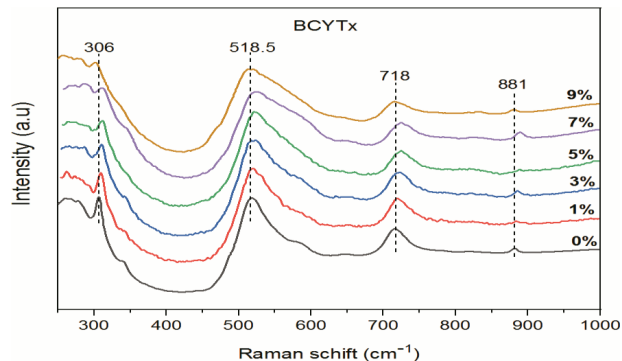Fig. 4.   Raman spectra at RT for the BCYT*x* samples.

(a)

(b)

(c)

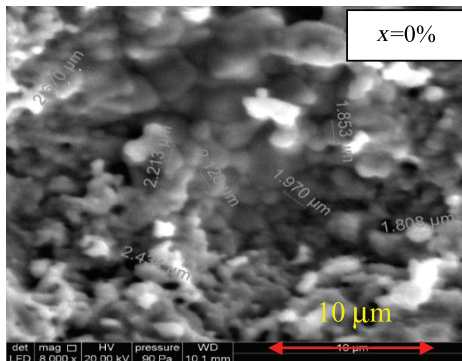Fig. 5.   (a)–(c) SEM images of BCYT*x* samples ($x = 0\%$, 5% and 9%).

and 9%) samples are displayed in Fig. 4. They show a narrow band at 306 cm^{-1} associated with [B$_1$, E(LO,TO)] mode, and two wide bands at 518.5 cm^{-1} and 718 cm^{-1} associated respectively with A$_1$(TO$_3$) and [A$_1$(LO$_3$), E(LO)] modes. Another band associated with A$_{1g}$ mode is present around 881 cm^{-1}. These Raman peaks observed in the samples are attributed to the peaks of the tetragonal phase.[20]

It is observed on these Raman spectra that as *x* increases ($x > 0\%$), the [B1, E(LO, TO)] mode tends to widen and decreases in intensity (Table 5), indicating a tendency towards the pseudo-cubic phase.[21] This result is in concordance with the above developed XRD results.
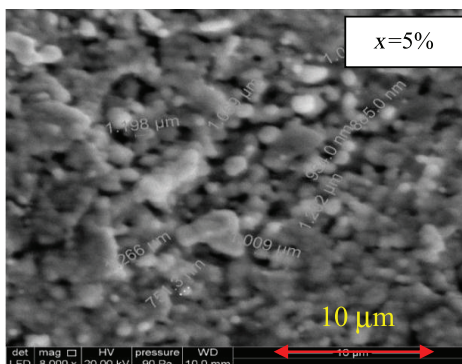
The presence of A$_{1g}$ mode can be attributed to the incorporation effect of Ce^{3+} and Y^{3+} in the BaTiO$_3$ matrix. Indeed, the A$_{1g}$ mode is inactive in Raman for simple perovskites with isovalent substituent as in Ba$_{1-x}$Sr$_x$TiO$_3$ ceramic developed by Dobal *et al.*[22] However, this mode becomes active when the Ba and/or Ti sites are substituted by an aliovalent substituent as observed by Liu *et al.* in (Ba$_{1-x}$Ce$_x$)(Ti$_{0.99}$Mn$_{0.01}$)O$_3$ ceramic using the solid-state reaction method calcined at 1250 °C for 4 h.[23]
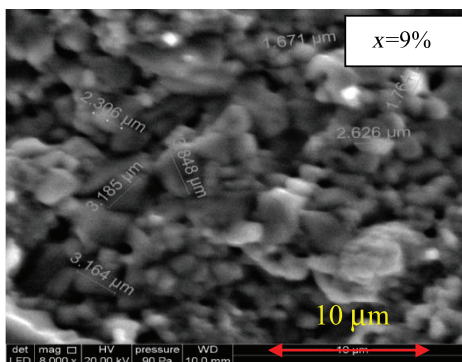
3.3.   *Microstructural analysis*

Figure 5 shows SEM images of three compositions of BCYT*x* ($x = 0\%$, 5% and 9%) samples sintered at 1200 °C/6 h.

Table 5.   FWHM and intensity ratio of [B$_1$, E(LO,TO)] mode.

	FWHM (cm^{-1})	Intensity
x (%)	[B$_1$, E(LO, TO)]	[B$_1$, E(LO,TO)]/[A$_1$(TO$_3$)]
0	7.42	1.02
1	8.10	0.93
3	8.88	0.91
5	9.04	0.85
7	9.28	0.83
9	9.35	0.80

Table 6.   Average grain size values of the as-prepared BCYT*x* samples.

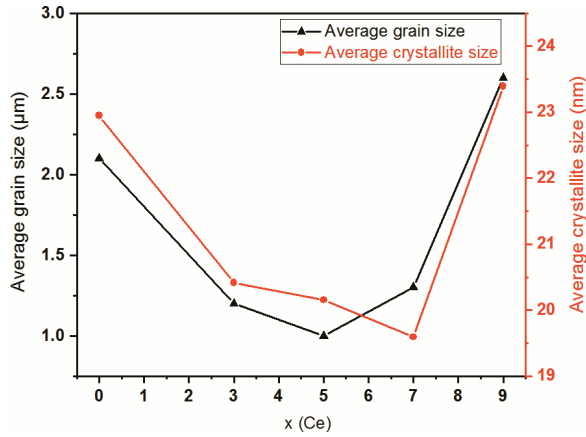| *x* (%)	Average grain size (µm)
0	2.1
3	1.2
5	1
7	1.3
9	2.6

Fig. 6.   Evolution of the average size of the crystallites and grains of BCYT*x* samples.

These images show the presence of grains of a regular morphology. Their average size is given in Table 6.

Figure 6 compares the evolution, as a function of cerium concentration, of the average crystallite size of BCYT*x* powders calcined at 950 °C (Table 4), and that of the average grain size (AGS) of BCYT*x* pellets sintered at 1200 °C

(Table 6). These parameters show a similar behavior with increasing concentration *x*; a decrease to *x* = 5–7%, followed by an increase. This decrease can be explained by the smaller ionic radius of cerium ($r(Ce^{3+}) = 1.34$ Å) compared to that of barium ($r(Ba^{2+}) = 1.61$ Å).

3.4. *Dielectric studies*

Figures 7(a)–7(f) illustrate the thermal variations of the permittivity (ε_r) of the BCYT*x* samples (*x* = 0%, 5% and 9%) at different frequencies.

The value of the maximum of the permittivity ($\varepsilon_{r\,max}$) at the FPT presents a particular behavior. Indeed, it decreases with frequency in the range 500 Hz–200 kHz and increases in the range 200 kHz–1 MHz for the undoped sample, whereas ($\varepsilon_{r\,max}$) corresponding to the doped samples decreases in the frequency range 500 Hz–50 kHz and increases in the range 50–700 kHz. This phenomenon has not been observed in $Ba_{1-x}Er_xTiO_3$[24] and $BaTi_{1-x}Y_xO_{3-x/2}$[25] ceramics with RE elements substituents. It can be pointed that the observed phenomenon is a manifestation of the resonance property observed in dielectric relaxor ceramics.[26]

Table 7 shows the evolution of the parameters $\varepsilon_{r\,max}$ and T_m of the BCYT*x* samples (*x* = 0%, 3%, 5%, 7% and 9%)
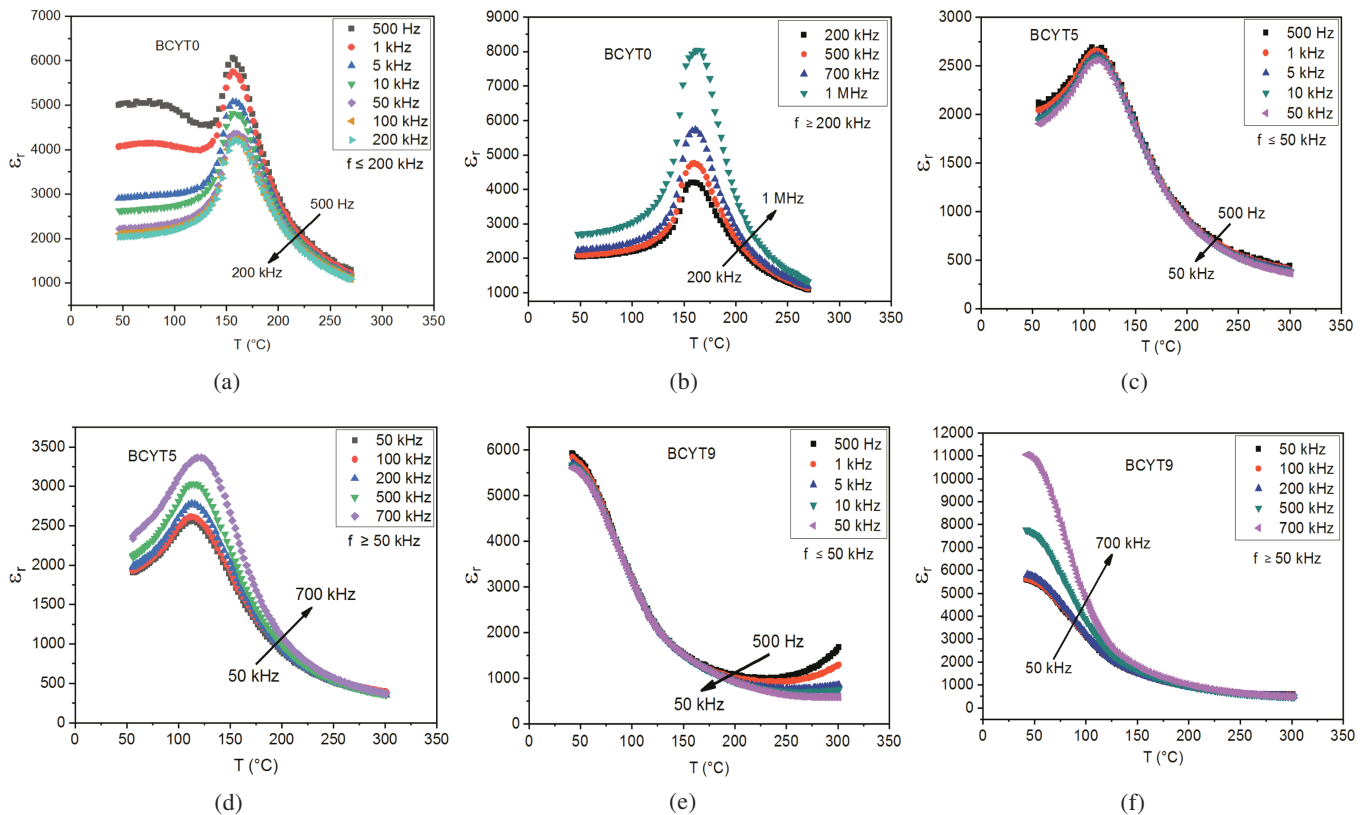

Fig. 7.   (a)–(f) Thermal variations of the permittivity of BCYT*x* (*x* = 0%, 5% and 9%).

Table 7. Values of the parameters $\varepsilon_{r\,max}$ and T_m at different frequencies.

f (kHz)	x (%)									
	0		3		5		7		9	
	$\varepsilon_{r\,max}$	T_m (°C)	$\varepsilon_{r\,max}$	T_m (°C)	$\varepsilon_{r\,max}$	T_m (°C)	$\varepsilon_{r\,max}$	T_m (°C)	$\varepsilon_{r\,max}$	T_m (°C)
0.5	6061	156	3478	135	2687	108	5051	91	>5927	<40
1	5747	156	3456	137	2655	111	5006	91	>5836	<40
5	5071	156	3430	137	2604	112	4935	91	>5706	<40
10	4815	156	3419	138	2587	112	4910	91	>5666	<40
50	4362	160	**3408**	138	**2559**	112	**4871**	93	**>5609**	<40
100	4237	160	3423	138	2612	113	4889	93	>5632	<40
200	**4203**	160	3507	138	2776	113	5032	93	>5819	<40
500	4752	160	4270	138	3032	116	6486	93	>7761	<40
700	5725	161	5582	138	3365	122	9086	93	>11056	<40

at different frequencies, where T_m is the temperature of the maximum of the permittivity at the FPT.

Higher values of $\varepsilon_{r\,max}$ were recorded and compared with those (at the frequency 100 kHz) of Yasmin *et al.*[27] who prepared $Ba_{1-x}Ce_xTiO_3$ ($x = 0\%$, 1%, 2%, 3% and 4%) samples using the conventional solid-state reaction method due probably to the method of preparation and the presence of Yttrium in our samples. It is observed that the parameter T_m (Table 7) depends on the frequency for all the BCYTx samples (presence of relaxation), and that the FPT has a clear diffuse character for the concentration $x = 5\%$ (Fig. 7(d)).

Moreover, it is observed from Fig. 8 that the maximum dielectric constant, $\varepsilon_{r\,max}$, first decreases and then increases with the increase of Ce content, and that this parameter follows the same evolution as that of the AGS (Table 6) and the density (Table 8) as a function of the Ce content. So, as the
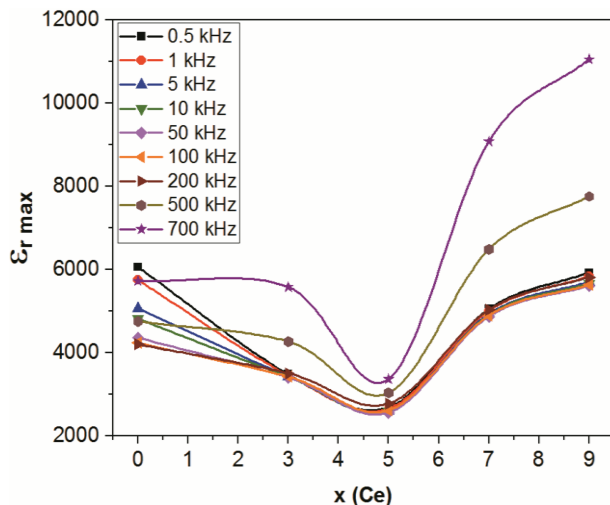
Table 8. Density values of the as-prepared BCYTx samples.

x (%)	Density (g/cm³)
0	5.16
3	4.5
5	3.81
7	4.84
9	5.38

material becomes denser, these dielectric properties become better.

Wang *et al.*[29] prepared $(1-x)[0.85BaTiO_3-0.15Bi(Mg_{2/3}-Nb_{1/3})O_3]-xNa_{0.5}Bi_{0.5}TiO_3$ ($x = 0$, 0.1, 0.2, 0.3, 0.4, 0.5, 0.6, 0.7, 0.8, 0.9, 1) samples via the solid-phase method, and have observed that $\varepsilon_{r\,max}$ increased from 1044 ($x = 0$) to 7269 ($x = 0.9$) and the AGS increased slightly from 0.98 μm ($x = 0$) to 1.32 μm ($x = 0.9$). Salhi *et al.*[30] prepared $Ba_{1-x}Ca_xTiO_3$ ($x = 0\%$, 1%, 5%, 10%, 15%, 20% and 30%) samples via the sol–gel method, and have also found that $\varepsilon_{r\,max}$ follows the same variation of the AGS as a function of the Ca content.

Table 9 shows the evolution of the parameter T_m at the frequency 1 kHz for all the BCYTx samples. It is observed that

Fig. 8. $\varepsilon_{r\,max}$ of BCYTx samples for all frequencies.

Table 9. Values of the temperature T_m at 1 kHz.

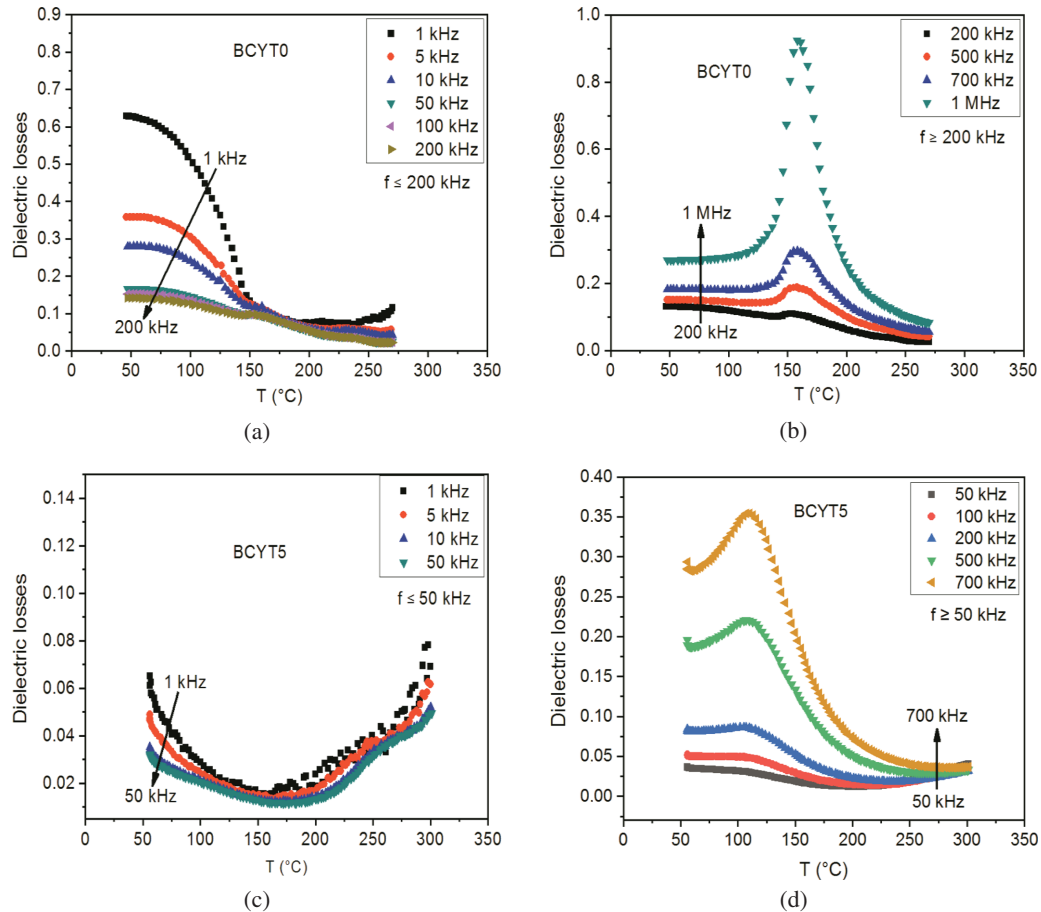| x (%)	T_m (°C)
0	156
3	137
5	111
7	91
9	<40

Fig. 9. (a)–(d) Thermal behavior of losses for BCYTx (x = 0% and 5%).

as x increases the parameter T_m decreases, and reaches a value that should be below 40 °C for the concentration $x = 9\%$.

Therefore, the incorporation of cerium results in a decrease of the temperature T_m of the $BaTi_{0.97}Y_{0.03}O_3$ sample. This result is consistent with those obtained by other preparation method performed by Yasmin *et al.*[27] and Xie *et al.*[28] who prepared $Ba_{1-x}Ce_xTiO_3$ ($x = 1\%$, 2%, 3% and 4%) samples using the solid-state reaction method sintered at 1400 °C for 6 h.

Figures 9(a)–9(d) illustrate the thermal behavior of losses for the BCYTx samples ($x = 0\%$ and 5%) at different frequencies.

Low dielectric loss values were recorded for all the BCYTx samples; these values show the same behavior in temperature and frequency as that observed for the permittivity (Fig. 7).

Figures 10(a)–10(d) illustrate the variations of the permittivity (ε_r) with frequency of the BCYTx samples ($x = 0\%$ and 7%) at different temperatures.

When the frequency increases for a given temperature, the permittivity increases and passes through a maximum, and then decreases and reaches its minimum value. This evolution is associated with the phenomenon of dielectric resonance followed by anti-resonance.

A similar behavior was observed in $Ba_{1-x}La_xTi_{(1-x/4)}O_3$[31] and $PbY_xTi_{1-x}O_3$[32] ceramics with RE elements substituents.

For the undoped sample BCYT0, the parameter $\varepsilon_{r\,max}$ moves towards the low frequencies when the temperature increases until 150 °C (Fig. 10(a)), while the displacement of $\varepsilon_{r\,max}$ is towards the high frequencies, for temperatures above 150 °C (Fig. 10(b)). The temperature at which the direction of displacement of $\varepsilon_{r\,max}$ is changed depends on the cerium concentration of the BCYTx samples (Figs. 10(c) and 10(d)), this temperature decreases as the cerium concentration increases. Indeed, as evidenced by Fig. 11, the resonance frequency (f_r) decreases first to reach a minimum value at the transition temperature, and then increases for all the BCYTx samples. There are two regions in the resonance frequency plot: the first region observed at low temperatures ($T < T_c$) is attributed to the ferroelectric phase (Figs. 10(a) and 10(c)), and the second region that occurs at higher temperatures ($T > T_c$) is attributed to the paraelectric phase (Figs. 10(b) and 10(d)). It is then concluded that cerium lowers the FPT temperature of the $BaTi_{0.97}Y_{0.03}O_3$ sample. This result confirms that obtained previously (Table 9).
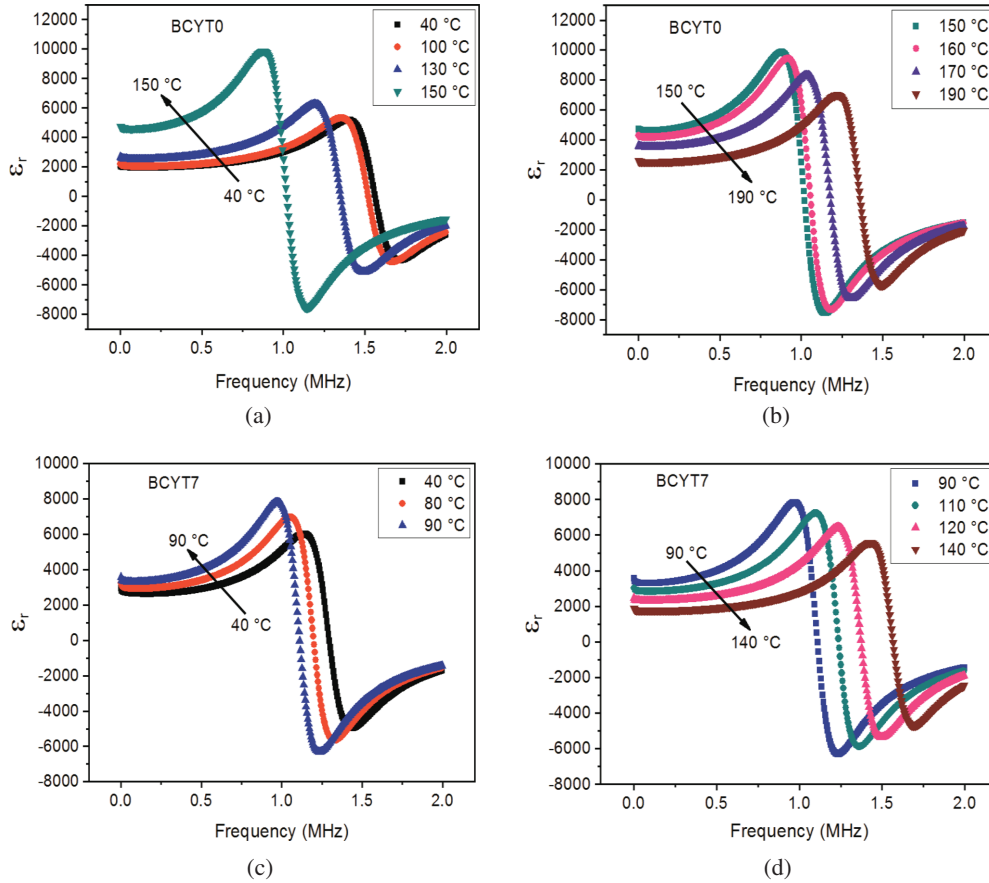
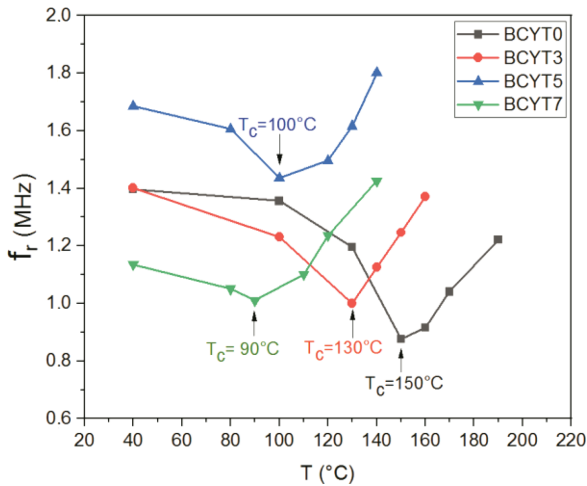Fig. 10.   (a)–(d) Variations of permittivity with frequency of BCYTx ($x = 0\%$ and 7%).

Fig. 11.   Thermal variations of the resonance frequency of BCYTx ($x = 0\%$, 3%, 5% and 7%).

4. Conclusion

A series of Ce-doped BaTi$_{0.97}$Y$_{0.03}$O$_3$ samples with the compositions (Ba$_{1-x}$Ce$_x$)(Ti$_{(0.97-x/4)}$Y$_{0.03}$)O$_3$ ($x = 0\%$, 1%, 3%, 5%, 7% and 9%) were prepared using the sol–gel process and were calcined at 950 °C for 4 h. Structural analysis showed

that all the samples crystallize in the pseudo-cubic structure with the presence of BaCeO$_3$ secondary phase for concentrations greater than 3%, Ce^{3+} ions incorporated Ba sites until $x = 7\%$ indicating that this concentration represents a solubility limit of Ce^{3+} ions in BaTi$_{0.97}$Y$_{0.03}$O$_3$. This behavior can be related to the minimum value of the AGS recorded for a concentration close to 7% as observed from SEM images. Raman spectroscopy analysis showed the appearance of the A$_{1g}$ mode, which we attribute to the incorporation effect of Ce^{3+} and Y^{3+} in the BaTiO$_3$ matrix. Dielectric measurements showed that the value of the maximum of the permittivity $\varepsilon_{r\,max}$ at the FPT of all the doped samples presents a particular behavior. Indeed, it decreases with frequency in the range 500 Hz–50 kHz and increases in the range 50–700 kHz. Also, the incorporation of cerium results in a decrease of the temperature of the maximum of the permittivity at the FPT of the BaTi$_{0.97}$Y$_{0.03}$O$_3$ sample. Moreover, the behavior of the permittivity as a function of frequency indicates the presence of the phenomenon of dielectric resonance in all the samples.

References

[1] D. Hennings, M. Klee and R. Waser, Advanced dielectrics: Bulk ceramics and thin films, *J. Adv. Mater.* **3**, 334 (1991).

2 S. F. Wang and G. O. Dayton, Dielectric properties of fine-grained barium titanate based X7R materials, *J. Am. Ceram. Soc.* **82**, 2677 (1999).

3 L. Zhou, P. M. Vilarinho and J. L. Baptista, Dependence of the structural and dielectric properties of $Ba_{1-x}Sr_xTiO_3$ ceramic solid solutions on raw material processing, *J. Eur. Ceram. Soc* **19**, 2015 (1999).

4 H. Kishi, N. Kohzu, J. Sugino, H. Ohsato, Y. Iguchi and T. Okuda, The effect of rare-earth (La, Sm, Dy, Ho and Er) and Mg on the microstructure in $BaTiO_3$, *J. Eur. Ceram. Soc* **19**, 1043 (1999).

5 S. Anwar, P. R. Sagdeo and N. P. Lalla, Crossover from classical to relaxor ferroelectrics in $BaTi_{1-x}Hf_xO_3$ ceramics, *J. Phys.: Condens. Matter* **18** (13), 3455 (2006).

6 Q. M. Sun, Q. L. Gu, K. J. Zhu, J. Wang and J. H. Qiu, Stabilized temperature-dependent dielectric properties of Dy-doped $BaTiO_3$ ceramics derived from sol-hydrothermally synthesized nanopowders, *Ceram. Int.* **42**, 3170 (2016).

7 D. Y. Lu and M. Toda, High-permittivity double rare-earth-doped barium titanate ceramics with diffuse phase transition, *J. Am. Ceram. Soc.* **89**, 3112 (2006).

8 M. Ganguly, S. K. Rout, W. S. Woo, C. W. Ahn and I. W. Kim, Characterization of A-site deficient samarium doped barium titanate, *Physica B* **411**, 26 (2013).

9 Z. Yao, H. Liu, Y. Liu, Z. Wu, Z. Shen, Y. Liu and M. Cao, Structure and dielectric behavior of Nd-doped $BaTiO_3$ perovskites, *Mater. Chem. Phys.* **109**, 475 (2008).

10 M. M. Vijatovic, B. D. Stojanovic, J. D. Bobic, T. Ramoska and P. Bowen, Properties of lanthanum doped $BaTiO_3$ produced from nanopowders, *Ceram. Int.* **36**, 1817 (2010).

11 F. D. Morrison, D. C. Sinclair and A. R. West, Electrical and structural characteristics of lanthanum-doped barium titanate ceramics, *J. Appl. Phys.* **86**, 6355 (1999).

12 Y. Liu and A. R. West, Ho-doped $BaTiO_3$: Polymorphism, phase equilibria and dielectric properties of $BaTi_{1-x}Ho_xO_{3-x/2}$: $0 \leq x \leq 0.17$, *J. Eur. Ceram. Soc.* **29**, 3249 (2009).

13 R. A. Eichel, Defect structure of oxide ferroelectrics-valence state, site of incorporation, mechanisms of charge compensation and internal bias fields, *J. Electroceram.* **19**, 11 (2007).

14 C. L. Freeman, J. A. Dawson , H. R. Chen, J. H. Harding, L. B. Ben and D. C. Sinclair, A new potential model for barium titanate and its implications for rare-earth doping, *J. Mater. Chem.* **21**, 4861 (2011).

15 Y. Tsur and C. A. Randall, Site occupancy of rare-earth cations in $BaTiO_3$, *Jpn. J. Appl. Phys.* **40**, 255 (2001).

16 J. Zhi, A. Chen, Y. Zhi, P. M. Vilarinho and J. L. Baptista, Incorporation of yttrium in barium titanate ceramics, *J. Am. Ceram. Soc.* **82**(5), 1345 (1999).

17 Y. Tsur, T. D. Dunbar and C. A. Randall, Crystal and defect chemistry of rare-earth cations in $BaTiO_3$, *J. Electroceram.* **7**, 25 (2001).

18 Y. Mizuno, H. Kishi, K. Ohnuma, T. Ishikawa and H. Ohsato, Effect of site occupancies of rare earth ions on electrical properties in Ni-MLCC based on $BaTiO_3$, *J. Eur. Ceram. Soc.* **27**(13), 4017 (2007).

19 D.-Y. Lu and D.-D. Han, In-situ diffuse phase transition at the curie point of $BaTiO_3$ induced by amphoteric Ce^{3+}/Ce^{4+} ions, *Ceram. Int.* **39**, 9727 (2013).

20 G. Burns, Lattice modes in ferroelectric perovskites. II. $Pb_{1-x}Ba_xTiO_3$ including $BaTiO_3$, *Phy. Rev. B* **10**, 1951 (1974).

21 M. Ganguly, S. K. Rout, T. P. Sinha, S. K. Sharma, H. Y. Park, C. W. Ahn and I. W. Kim, Characterization and rietveld refinement of A-site deficient lanthanum doped barium titanate, *J. Alloys Compd.* **579**, 473 (2013).

22 P. S. Dobal, A. Dixit, R. S. Katiyar, D. Garcia, R. Guo and A. S. Bhalla, Micro-Raman study of $Ba_{1-x}Sr_xTiO_3$ ceramics, *J. Raman Spectrosc.* **32**, 147 (2001).

23 S. Liu, Q. Xie, L. Zhang, Y. Zhao, X. Wang, P. Mao, J. Wang and X. Lou, Tunable electrocaloric and energy storage behavior in the Ce, Mn hybrid doped $BaTiO_3$ ceramics, *J. Eur. Ceram. Soc.* **38**(14), 4664 (2018).

24 Y. Leyet, R. Peña, Y. Zulueta, F. Guerrero, J. Anglada-Rivera, Y. Romaguera and J. Perez de la Cruz, Phase transition and PTCR effect in erbium doped BT ceramics, *Mater. Sci. Eng.: B* **177**(11), 832 (2012).

25 X. Wang, P. Ren, Q. Wang, H. Fan and G. Zhao, Dielectric, piezoelectric and conduction properties of yttrium acceptor-doped $BaTiO_3$ ceramics, *J. Mater. Sci: Mater. Electron.* **27**, 11762 (2016).

26 S. Mahboob, Rizwana, G. Prasad and G. S. Kumar, Simulation of dielectric and resonance and anti-resonance data using modified Lorentz equation (T and ω simultaneously) of relaxor ferroelectric and piezoelectric ceramics, *Bull. Mater. Sci.* **42**, 56 (2019).

27 S. Yasmin, S. Choudhury, M. A. Hakim, A. H. Bhuiyan and M. J. Rahman, Effect of cerium doping on microstructure and dielectric properties of $BaTiO_3$ ceramics, *J. Mater. Sci. Technol.* **27**(8), 759 (2011).

28 S. Xie, Y. Bai, F. Han, S. Qin, J. Li, L. Qiao and D. Guo, Distinct effects of Ce doping in A or B sites on the electrocaloric effect of $BaTiO_3$ ceramics, *J. Alloys Compd.* **724**, 163 (2017).

29 T. Wang, J. Liu, L. Kong, H. Yang, F. Wang and C. Li, Evolution of the structure, dielectric and ferroelectric properties of $Na_{0.5}Bi_{0.5}TiO_3$-added $BaTiO_3$-$Bi(Mg_{2/3}Nb_{1/3})O_3$ ceramics, *Ceram. Int.* **46**, 25392 (2020).

30 A. Salhi, S. Sayouri, B. Jaber and L. Omari, Effect of microwaves on the synthesis, structural and dielectric properties of Ca-modified $BaTiO_3$ ceramics, *Appl. Phys. A* **124**, 389 (2018).

31 A.ElGhandouri,S.Sayouri,T.LamcharfiandA.Elbasset,Structural, microstructural and dielectric properties of $Ba_{1-x}La_xTi_{(1-x/4)}O_3$ prepared by sol gel method, *J. Adv. Dielect.* **9**(3), 1950026 (2019).

32 M. Belhajji, S. Sayouri, A. Nfissi and T. Lamcharfi, Effect of the occupation of Pb and Ti sites on the structural, microstructural and dielectric properties of Y-doped $PbTiO_3$ samples, *J. Mater. Sci.: Mater. Electron.* **30**(12), 16065 (2019).